Energy Equip. Sys./ Vol. 8/No. 2/June 2020/ 111-126

ENERGY EQUIPSYS

Energy Equipment and Systems

http://energyequipsys.ut.ac.ir
www.energyequipsys.com

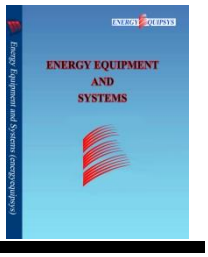

Interaction of laminar natural convection and radiation in an inclined square cavity containing participating gases

Authors

Maryam Moein Addini [a]
S.Abdolreza Gandjalikhan Nassab[a*]

[a] Mechanical Engineering Department, School of Engineering, Shahid Bahonar University of Kerman, Kerman, Iran

Article history:

Received : 23 February 2019
Accepted : 14 April 2019

ABSTRACT

Two-dimensional numerical study of flow and temperature fields for laminar natural convection and radiation in the inclined cavity is performed in the present work. The walls of the square cavity are assumed kept at constant temperatures. An absorbing, emitting, and scattering gray medium is enclosed by the opaque and diffusely emitting walls. The set of governing equations, including conservation of mass, momentum, and energy for fluid flow, is solved numerically by the CFD method, while radiation computation is based on the numerical solution of the radiative transfer equation. The finite volume method has been adopted to solve the governing equations, and the discrete ordinates method (DOM) is used to model the radiative transfer in the absorbing-emitting medium. The effects of Rayleigh number from 10^3 to 10^6 and inclination angle in a broad range from 0 to 90^o on temperature and velocity distributions and Nusselt numbers are investigated. It was found that the total heat transfer in the cavity is increased under thermal radiation, and variation of inclination angle causes a sweep behavior in the flow pattern inside the cavity.

Keywords: Laminar Natural Convection Flow, Inclined Cavity, Radiation, DOM.

1. Introduction

Combined natural convection and radiation in differentially heated enclosures are important in many areas such as building systems, fire spreading and collectors, etc. Therefore, studies on this topic have been carried out over the past several decades. Various pure natural convection problems have been carried out numerically and experimentally by many researchers. Reviews on this subject can be found in the publication of Vahal Davis and Jones [1], Ostrach [2-3], Barakos et al. [4], Markatos et al. [5] and Fusegi et al. [6]. Reviewing the preceding investigations shows that several works are found for the problem of combined radiation and natural convection in participating media.

Chang et al. [7] investigated combined radiation and natural convection in square enclosures with partitions mounted at the ceiling and floor midpoint. Webb and Viskanta [8] carried out a numerical study of coupled heat transfer problems involving both convection and radiation in a rectangular cavity. The combined natural convection with radiation heat transfer in enclosures was

* Corresponding author: S.Abdolreza Ganjalikhan Nasab
Mechanical Engineering Department, School of Engineering, Shahid Bahonar University of Kerman, Kerman, Iran
Email: ganj110@uk.ac.ir

studied by Yang [9]. Yucel et al. [10] used the discrete ordinate method to study combined natural convection and radiation heat transfer in a rectangular participating medium. Lauriant [11-12] computed interaction between natural convection and radiation in rectangular enclosures using the P-1 differential approximation to represent radiative heat transfer. Tan and Howell [13] studied the benchmark problem of the square cavity for solving combined radiation and thermal convection in two-dimensional square participating media. A numerical investigation of combined natural convection and radiation heat transfer with a gray and scattering medium has been performed using the hybrid thermal lattice Boltzmann method by Moufekkir et al. [14]. Lari et al. [15] analyzed the effect of radiative heat transfer on natural convection heat transfer in a square cavity under ordinary room conditions. Colomer et al. [16], have studied the combined natural convection and radiation in a three-dimensional heated cavity by using DOM to solve the RTE. Capdevila et al. [17-19], Ibrahimi [20] analyzed the effect of surface and gas radiation on turbulent natural convection in 3D and 2D cavities. Baytas [21], Oztop [22], Varal et al. [23] performed a computational study on laminar natural convection in inclined enclosures. Bouali et al. [24] analyzed the effects of surface radiation and inclination angle on the heat transfer and flow structures in an inclined rectangular cavity. Ahmed et al. [25] presented a computational study of the radiation-natural convection in an inclined porous cavity with corner heater. Mezrhab et al. [26-27] carried out a numerical study of the radiation-natural convection interaction in a square cavity with a heat-generating conducting body. They found that the streamlines and isotherms structures are strongly affected by the thermal radiation heat transfer. The effects of surface radiation and number partition on heat transfer and flow structures in a rectangular enclosure, under an inclined angle of 45° are studied by Rabhi et al. [28]. The authors [29] investigated the interaction effect between mixed convection and volumetric radiation in the tilted lid-driven cavity

In all of the above research works, the problem of combined natural convection with radiation in a participating media inside an inclined square cavity has not been studied. Therefore, the purpose of the present study is to investigate the effects of thermal radiation on thermohydrodynamics behavior of an inclined cavity containing radiating gas. To achieve this goal, the radiative transfer equation is solved using the conventional DOM, and the finite volume method [30] has been adopted to solve the other governing equations.

Nomenclature

A_x , A_y	areas of control volume face normal to the x and y-directions, respectively (m^2)
C_p	specific heat (J/kgK)
g	gravitational acceleration (ms^{-2})
I	radiation intensity (W/m^2)
I^*	dimensionless radiation intensity
I_b	black body radiation intensity(W/m^2)
k	thermal conductivity($Wm^{-1}K^{-1}$)
L	cavity depth or width (m)
Nu_c	convective Nusselt number
Nu_r	radiative Nusselt number
Nu_t	total Nusselt number
n_w	outward unit vector normal to the surface
p	Pressure ($N.m^{-2}$)
P	dimensionless pressure
Pr	Prandtl number, υ/α

2. Mathematical Formulation

The studied geometry, as shown in Fig. 1 is an inclined square cavity by isothermal walls at different temperatures T_h and T_c ($T_h > T_c$). It is assumed that laminar natural convective and thermal radiative heat transfers occur simultaneously. The temperature difference between the top wall (T_c) and other walls (T_h) generates a temperature gradient in the fluid, and the consequent density difference induces a fluid motion. All physical properties in the system are assumed to be constant, except for the density in the buoyancy term, which follows the Boussinesq approximation. The viscous dissipation term in the energy

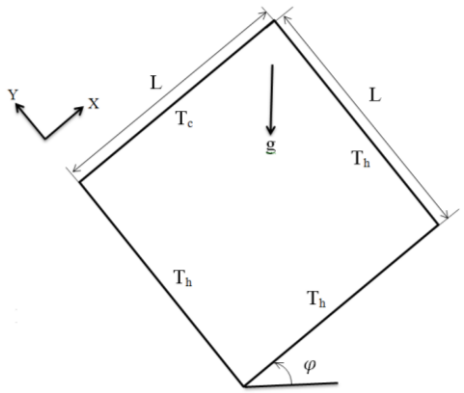

Fig.1: Geometry of the inclined enclosure

equation assumed to be neglected. The medium in the system is assumed to be gray, and the emissivities of the walls are also assumed to be constant.

The present study reports the computations with a board range of Rayleigh number (10^3-10^6) and inclination angle ($0 \leq \varphi \leq 90°$). Results are presented in terms of the streamline and isotherm plots in the cavity and the distributions of convective, radiative, and total Nusselt numbers at the bottom wall.

2.1 Governing Equations

The flow is assumed to be incompressible, laminar, and two dimensional in a square cavity with inclination angle φ respect to the horizontal axis. The governing equations, including conservations of mass, momentum, and energy can be written as follows:

Continuity: $$\frac{\partial u}{\partial x}+\frac{\partial v}{\partial y}=0 \quad (1)$$

x- momentum (2)

$$u\frac{\partial u}{\partial x}+v\frac{\partial u}{\partial y}=-\frac{1}{\rho}\frac{\partial p}{\partial x}+\upsilon\left(\frac{\partial^2 u}{\partial x^2}+\frac{\partial^2 u}{\partial y^2}\right)+g\,\beta(T-T_c)sin\varphi$$

y- momentum (3)

$$u\frac{\partial v}{\partial x}+v\frac{\partial v}{\partial y}=-\frac{1}{\rho}\frac{\partial p}{\partial y}+\upsilon\left(\frac{\partial^2 v}{\partial x^2}+\frac{\partial^2 v}{\partial y^2}\right)+g\,\beta(T-T_c)cos\varphi$$

Energy (4)

$$u\frac{\partial T}{\partial x}+v\frac{\partial T}{\partial y}=\alpha\left(\frac{\partial^2 T}{\partial x^2}+\frac{\partial^2 T}{\partial y^2}\right)-\frac{1}{\rho c_p}\nabla.q_r$$

The radiative source term in the energy equation, is evaluated by solving the radiative transfer equation (RTE). The local divergence of the radiative flux $\nabla.q_r$ can be calculated as shown by Modest [31]:

$$\nabla.q_r=\sigma_a(4\pi I_b(\vec{r})-\int_{4\pi} I(\vec{r},\vec{s})\,d\Omega) \quad (5)$$

In the above equation,σ_a is the absorption coefficient, $I(\vec{r},\vec{s})$ is the radiation intensity at position r and in the direction s, and $I_b(\vec{r})=\sigma(T(\vec{r}))^4/\pi$ is the black body radiation intensity. It is necessary to solve the radiative transfer equation to obtain the radiation intensity field and $\nabla.q_r$. For an absorbing, emitting, and scattering gray medium RTE can be written as [31]:

$$s.\nabla I(\vec{r},\vec{s})=\sigma_a(\vec{r})I_b(\vec{r})-\beta(\vec{r})I(\vec{r},\vec{s})+\frac{\sigma_s(\vec{r})}{4\pi}\int_{4\pi} I(\vec{r},\vec{s'})\phi(\vec{r},\vec{s},\vec{s'})d\Omega' \quad (6)$$

in which σ_s is the scattering coefficient, $\beta=\sigma_s+\sigma_a$ the extinction coefficient, and $\phi(\vec{r},\vec{s},\vec{s'})$ is the scattering phase function for the radiation from incoming direction s' and confined within the solid angle $d\Omega'$ to scattered direction s confined within the solid angle $d\Omega$. In this study, the isotropic scattering medium is considered, in which the scattering phase function is equal to unity. The boundary condition for a diffusely emitting and reflecting gray wall is

$$I(\vec{r}_w,\vec{s})=\varepsilon(\vec{r}_w)I_b(\vec{r}_w)+\frac{(1-\varepsilon_w)}{\pi}\int_{\vec{n}_w.\vec{s}'<0} I(\vec{r}_w,\vec{s})\left|\vec{n}_w.\vec{s}'\right|d\Omega' \quad \vec{n}_w.\vec{s}>0 \quad (7)$$

where ε_w is the wall emissivity, $I_b(\vec{r}_w)$ is the black body radiation intensity at the temperature of the boundary surface, and n_w is the outward unit vector normal to the surface. For Eqs. (1) to (4), the no-slip boundary condition is employed for momentum equations, and for energy equation, the fluid temperature at the isotherm solid surfaces are kept equal to wall temperature, which are considered T_c and T_h on cold and hot surfaces, respectively.

2.2 Radiative Transport Equation

In this study, the discrete ordinate method (DOM) has been adopted to solve the RTE (Eq. 6) using S_4 approximation. In this method, the RTE is substituted by a set of M discrete equations for a finite number of directions Ω_m, and each integral is substituted by a quadrature series. By this technique, the RTE becomes as follows:

$$(\Omega_m.\nabla)I(r,\Omega_m) = -\beta I(r,\Omega_m) + \sigma_a I_b(r) + \frac{\sigma_s}{4\pi}\sum_{k=1}^{M} w_k\, I(r,\Omega_k)\emptyset(\Omega_m,\Omega_k) \quad (8)$$

subject to the boundary condition:

$$I(r_w,\Omega_m) = \epsilon I_b(r) + \frac{(1-\varepsilon)}{\pi}\sum_{n.,\Omega_k<0} w_k\, I(r_w,\Omega_k)|n.\Omega_k| \quad (9)$$

where w_k is the ordinate weight. This angular approximation transforms the original equation into a set of coupled differential equations. In Cartesian coordinates, Eq. (8) becomes:

$$\xi_m\frac{\partial I_m}{\partial x} + \eta_m\frac{\partial I_m}{\partial y} + \beta I_m = \beta S_m \quad (10)$$

where S_m is a shorthand for the radiative source function that can be calculated by the following equation:

$$S_m = (1-\omega)I_b(r) + \frac{\omega}{4\pi}\sum_{k=1}^{M} w_k\, I(r,\Omega_k)\emptyset(\Omega_m,\Omega_k) \quad (11)$$

in which ω is the albedo coefficient, $\omega = \sigma_s/\beta$. By the finite volume method, the following equation can be obtained for computing the radiant intensity for central nodes at each control volumes [31]:

$$I_{pi} = \frac{|\xi_i|A_x I_{xi} i + |\eta_i|A_y I_{yi} + S_{pi}}{\beta\forall + |\xi_i|A_x + |\eta_i|A_y} \quad (12)$$

in which ξ_i, η_i are the directional cosines for the direction S_m and $\forall$ is the element of cell volume. For the radiative boundary conditions, all walls are assumed to emit and reflect diffusely with constant wall emissivity ε_w =0.8.

2.3. Non-dimensional Forms of the Governing Equations

In numerical solution of the set of governing equations, including the continuity, momentum, and energy, the following dimensionless parameters are used to obtain the non-dimensional forms of these equations.

$$X = \frac{x}{L},\ Y = \frac{y}{L},\ U = \frac{uL}{\alpha},\ V = \frac{vL}{\alpha},\ P = \frac{pL^2}{\rho\alpha^2}$$

$$\tau = \beta L,\ (1-\omega) = \frac{\sigma_a}{\beta},\ RC = \frac{\sigma L T_h^3}{k}$$

$$I^* = \frac{I}{\sigma T_h^4},\ S^* = \frac{S}{\sigma T_h^4},\ q_r^* = \frac{q_r}{\sigma T_h^4}$$

$$\Theta = \frac{T-T_c}{T_h-T_c},\ \theta_1 = \frac{T_c}{T_h-T_c}$$

$$\theta_2 = \frac{T_h}{T_c},\ Ra = \frac{g\beta(T_h-T_c)L^3}{\upsilon\alpha},\ Pr = \frac{v}{\alpha}$$

after invoking the Boussinesq approximation and neglecting the viscous dissipation, The governing equations for laminar steady two-dimensional natural convection can be expressed in the dimensionless forms as:

$$\frac{\partial U}{\partial X} + \frac{\partial V}{\partial Y} = 0 \quad (13)$$

$$U\frac{\partial U}{\partial X} + V\frac{\partial U}{\partial Y} = -\frac{\partial P}{\partial X} + Pr\left(\frac{\partial^2 U}{\partial X^2} + \frac{\partial^2 U}{\partial Y^2}\right) + Ra\ Pr\Theta\sin\varphi \quad (14)$$

$$U\frac{\partial V}{\partial X} + V\frac{\partial V}{\partial Y} = -\frac{\partial P}{\partial Y} + Pr\left(\frac{\partial^2 V}{\partial X^2} + \frac{\partial^2 V}{\partial Y^2}\right) + Ra\ Pr\Theta\cos\varphi \quad (15)$$

$$U\frac{\partial \Theta}{\partial X} + V\frac{\partial \Theta}{\partial Y} = \quad (16)$$

$$\left(\frac{\partial^2\Theta}{\partial X^2}+\frac{\partial^2\Theta}{\partial Y^2}\right)-\tau(1-\omega)\mathrm{RC}\theta_1\theta_2\left[\frac{4}{\theta_2^4}\left(\frac{\Theta}{\theta_1}+1\right)^4-\sum_{k=1}^{M}I_k^*w_k\right]$$

The velocity and temperature boundary conditions have the following dimensionless forms:

at X=0 and X=1 U=V=0 and $\Theta = 1$
at Y=0 U=V=0 and $\Theta = 1$
at Y=1 U=0, V=0 and $\Theta = 0$

The convective, radiative and total Nusselt number at the walls can be calculated as follows:

$$Nu_c = \frac{q_c L}{k\Delta T} = -\frac{\partial\Theta}{\partial Y} \quad (17)$$

$$Nu_r = \frac{q_r L}{k\Delta T} = RC.\theta_1.\theta_2\, q_r^* \quad (18)$$

$$Nu_t = Nu_c + Nu_r = -\frac{\partial\Theta}{\partial Y} + RC.\theta_1.\theta_2\, q_r^* \quad (19)$$

$$\overline{Nu} = \frac{1}{A}\int_A Nu\, dA \quad (20)$$

3. Numerical Method

The set of governing equations are integrated over the control volumes, which produces a set of algebraic equations. The SIMPLE algorithm is used to solve the coupled system of governing equations. The discrete procedure utilizes the line-by-line method connected to the finite volumes technique with the Hybrid technique [32] for the calculations of convective terms at the faces of control volumes, and central differencing is used to discretize the diffusion terms. These computations are coded into a computer program in FORTRAN. Since the buoyancy term appears in the flow equations and also the RTE depends on the temperature field through the emission term, all of the governing equations are solved simultaneously. Based on the result of grid tests for obtaining the grid-independent solutions, six different mesh sizes were used in the grid independence study. The corresponding maximum values of convective and radiative Nusselt numbers on the bottom wall of the cavity are calculated and tabulated in Table 1. The grid-independence study shows an optimum uniform grid size of 90×90 while using a denser mesh of 100×100 resulted in less than 1% difference in the value of Nusselt numbers on the bottom wall. Therefore, the grid size of 90×90 is sufficient for this simulation.

In this study, S4 approximation has been used to compute the divergence of radiative heat flux. In the computation of radiant intensity, the numerical solution of Eq. (10) can be started with the black body assumption for the boundaries by neglecting the source term Si. In the next iteration, the general forms of Eq. (12) and its boundary condition is applied. This procedure is repeated until the convergence criterion is met. Finally, from the radiative intensity obtained by Eq. (12), the divergence of radiative heat flux, which is needed for the numerical solution of the energy equation, can be calculated. The computation is terminated when the residuals for the continuity and momentum and energy equations become less than 10-4, with these criteria in the numerical solution of RTE, the maximum difference between the radiative intensities computed during two consecutive iteration levels did not exceed 10-6 at each nodal point. By this numerical strategy, the velocity, temperature, and radiation intensity distributions inside the flow domain can be obtained. It should be noted that the same optimum grid size 90×90 is also employed for radiation computations as a result of the grid-independent study done in the calculation of radiant intensity from RTE.

4. Code and Result Verifications

4.1 pure convection validation

In order to validate the convection part of the problem, the computational procedure has been solved without radiation and compared with the previous results in the literature. Comparisons of the average Nusselt number at the hot wall for a different Rayleigh numbers in a test case with two vertical isothermal walls and two horizontal adiabatic walls are shown in Table 2. As it is seen, a comparison between the present computations and results of other researchers shows a good agreement.

Table 1: Grid independence study
Ra=10^6, Pr=0.71, RC = 10, $\omega = 0.5, \tau = 0.01, \varphi = 0$

Grid size	The maximum value of convective Nusselt number	The maximum value of radiative Nusselt number
50 × 50	11.396	10.964
60 × 60	11.863	11.073
70 × 70	12.117	11.149
80 × 80	12.256	11.202
90 × 90	12.331	11.240
100 × 100	12.369	11.266

Table 2: Comparison of the computed average Nusselt number at the hot wall at different Ra

Ra	Current work	De Vahl Davis [1]	Barakos et al.[4]	Markatos & Pericleous [5]	Fusegi et al. [6]	Lari et al. [15]
10^3	1.126	1.118	1.114	1.108	1.134	1.122
10^4	2.191	2.243	2.245	2.201	2.274	2.244
10^5	4.516	4.519	4.510	4.430	4.568	4.518
10^6	9.045	8.799	8.806	8.754	8.935	8.814

4.2 Validation of combined conductive-radiative heat transfer results

To check the performance and accuracy of DOM and radiative computation, validation was performed by comparing the streamlines and isotherm contours for a case of combined convection–radiation cavity with isothermal walls performed by Byun and Hyuk Im [33]. In Figs. 2, 3, the streamlines and isotherm contours inside the enclosure obtained by the present computation are compared to those found in Ref. [33]. There is also a good consistency between those theoretical results. For another test case, the variation of temperature in the midplane of the enclosure along the horizontal axis is shown in Fig. 4 compared to that obtained by Mahapatra et al. [34].

In this test case, a square enclosure of length L, containing an absorbing, emitting, and scattering medium, is considered in which a combined conductive-radiative heat transfer takes place. The left wall of the enclosure is hot, and other walls are cold, with the nondimensional temperatures equal to 1 and 0.5, respectively. This problem solved numerically by Mahapatra et al. [34] using the DOM. There is also a good consistency between those theoretical results.

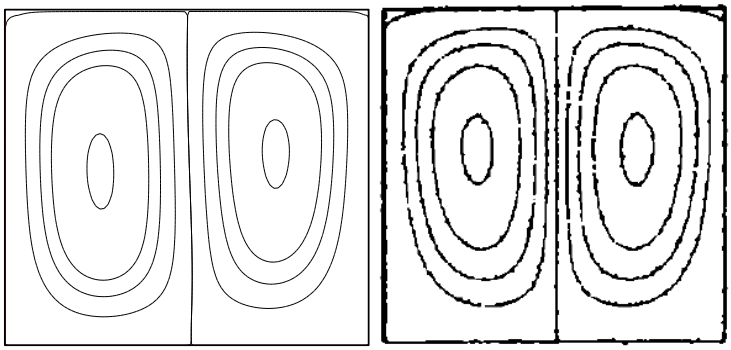

(a) : present study (b) : Byun and Hyuk Im [33]

Fig.2: Distribution of the streamlines
$Ra = 0.92 \times 10^6, Pr = 0.71, \tau = 1, \omega = 0$

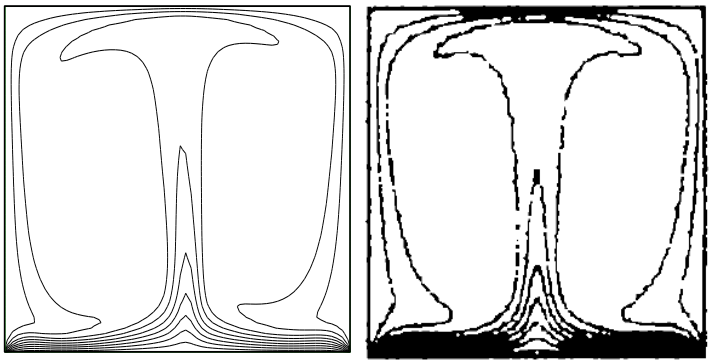

(a) : present study (b) : Byun and Hyuk Im [33]

Fig.3: Distribution of the isotherm contours

$Ra = 0.92 \times 10^6 . Pr = 0.71 . \tau = 1 . \omega = 0$

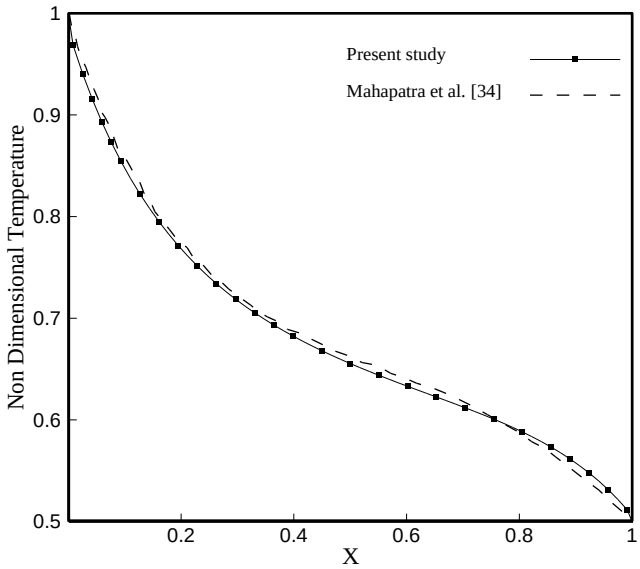

Fig.4: Comparison of the computed mid-plane temperature with the theoretical result by Mahapatra et al. [34]

RC = 10, $\omega = 0.5 . \varepsilon_w = 0.5 . \tau = 1$

5. Results and Discussions

The main concern of the present work is thermal and hydrodynamic analyses of a square cavity filled with isotropic scattering media, in which natural convection takes place because of hot and cold walls. All computations reported in this numerical study are performed with a uniform grid composed of 90×90 cells. It should be noted that the Prandtl number is fixed at Pr=1.0 and under the Boussinesq approximation which is employed in the numerical solution of momentum equations, the values of temperature ratios are chosen equal to $\theta_1 = \frac{T_c}{T_h - T_c} = 10 . \theta_2 = \frac{T_h}{T_c} = 1.1$. In this section, results are presented in the form of streamline and isotherm contour plots, Nusselt number distributions on the bottom wall of the cavity, and midplane velocity profiles. Besides, an attempt is made to carry out the effects of Rayleigh number and the cavity inclination angle on thermohydrodynamic characteristics of combined radiative-convective heat transfer in the square cavity.

5.1 Effect of Rayleigh number

To demonstrate the effects of Rayleigh number on flow and temperature distributions, the isotherms (left) and streamlines (right) are plotted in Fig. 5 for a wide range of Rayleigh numbers from 10^3 to 10^6, where the gas flow in natural convection is in the laminar regime.

From streamline plots, it is seen that in all cases, the flow is bicellular in which two

separate recirculated domains display in the left and right parts of the cavity. For small values of Ra, these two vortices have similar shapes, and there is symmetry about the midplane for the fluid flow. But, for large values of Rayleigh number, the flow rates in both recirculated zones increase, and the flow symmetry about the mid-plane is almost disappeared.

One can state from Fig. 5 that for low Rayleigh number, the isotherms indicate the existence of a conductive regime in which the left and right parts of the cavity have similar temperature distributions. By increasing Ra, the temperature distribution at the core of the

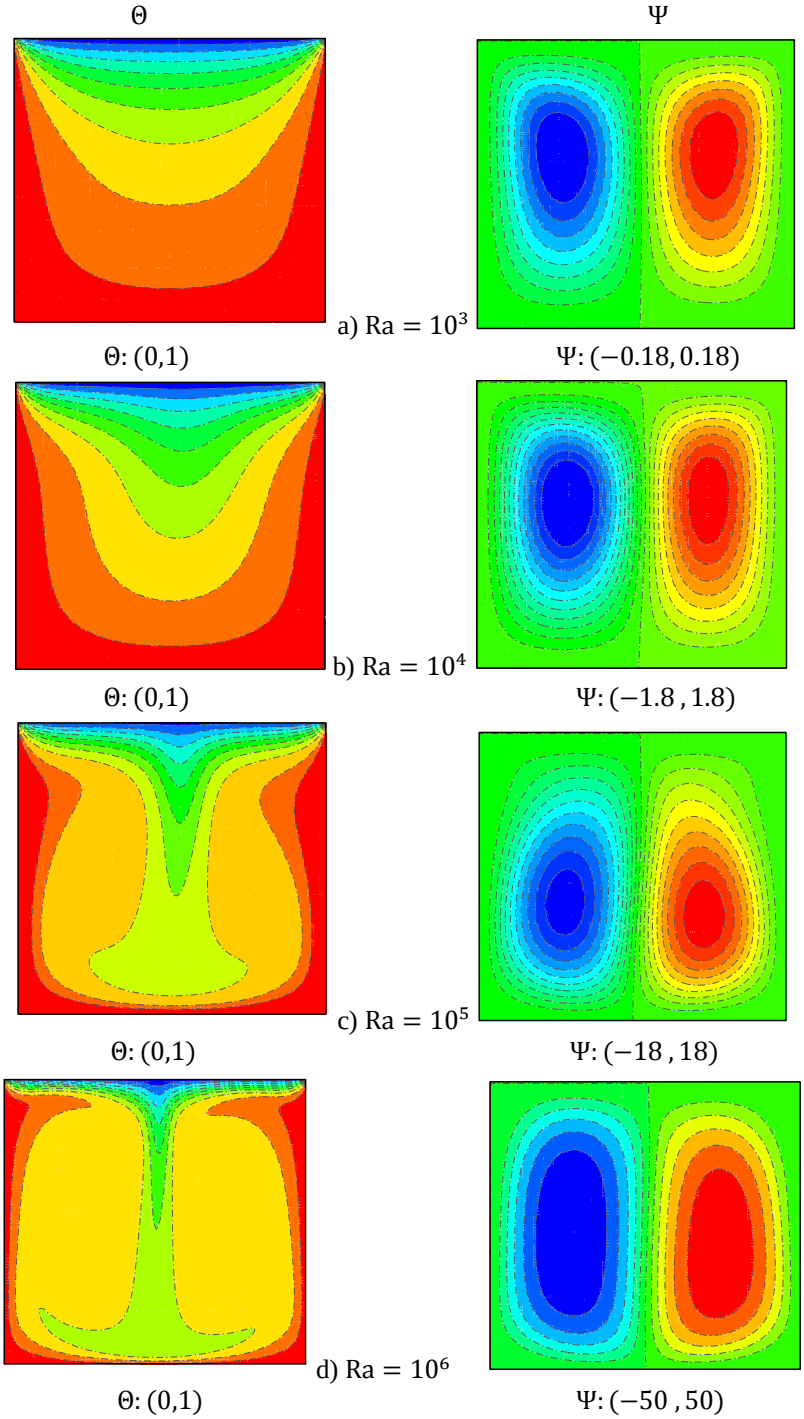

Fig.5: Streamlines (Ψ) and temperature (Θ) contour at different Rayleigh number for RC = 20, $\omega = 0.5. \tau = 0.1. \varphi = 0°$
(a) Ra = 10^3, (b) Ra = 10^4, (c) Ra = 10^5 (d) Ra = 10^6

cavity becomes more homogeneous because of convection effect, and more temperature gradients near the cavity hot walls take place that leads to a high rate of wall heat flux. The effects of the cavity inclination angle on both streamline, and isotherm distributions are studied in Fig. 6. It is seen that both fluid flow and thermal behaviors are much affected by variation in the inclination angle. Such that by increasing in φ from 0 to 15°, the symmetry in streamline distributions disappeared, and in the case of $\varphi = 15^{\circ}$ the main recirculated zone takes place on the right part of the cavity and a small one on the other hand. By further increasing in φ up to 45°, the flow becomes unicellular around the core of the cavity, and then for $\varphi = 60^{\circ}$ to 75° A sweep behavior is seen for the fluid flow. Finally, for the cavity with an inclination angle equal to $\varphi = 90^{\circ}$. a unicellular buoyant flow again appears with the center approached the right sense in the cavity. One can notice to this fact that different patterns for streamlines at different cavity inclination angle is due to variation in the direction of buoyancy force which is always in the opposite sense with gravity. The maximum rate of natural fluid flow takes place in the situation of hot walls down and cold ones at the upper. It is evident that these complex changes in streamline patterns because of the variation in cavity inclination angle lead to having different distributions for isotherms, as can be seen from Fig. 6.

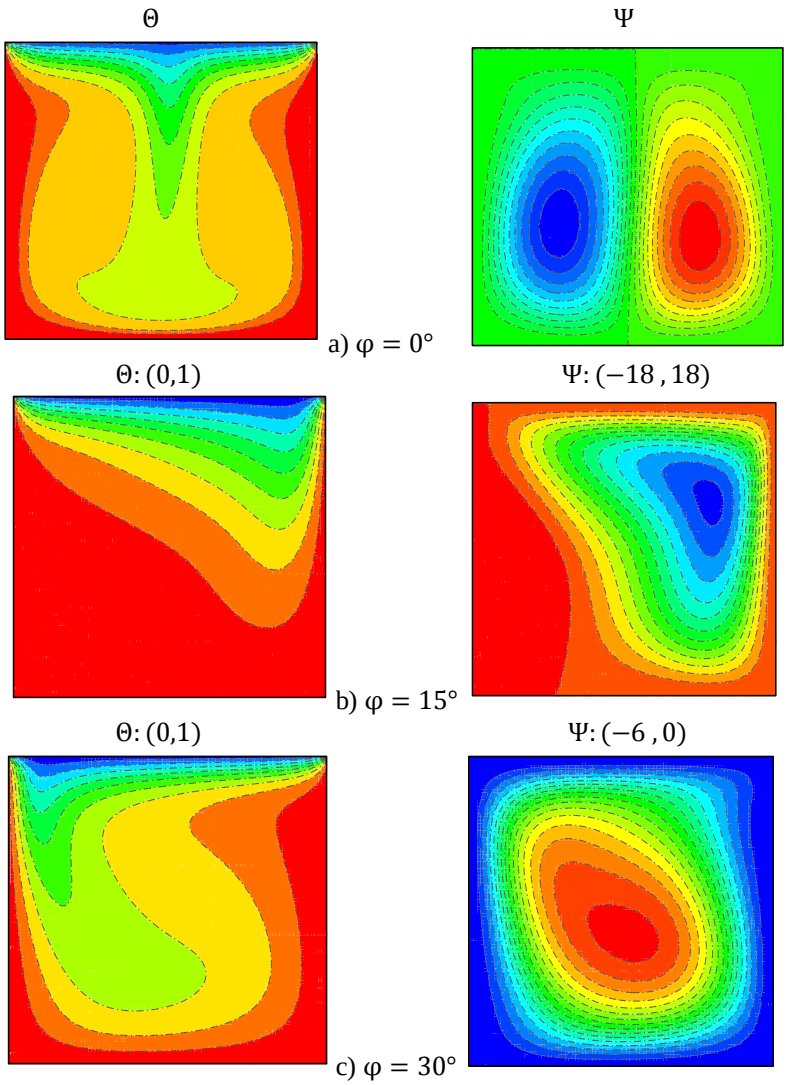

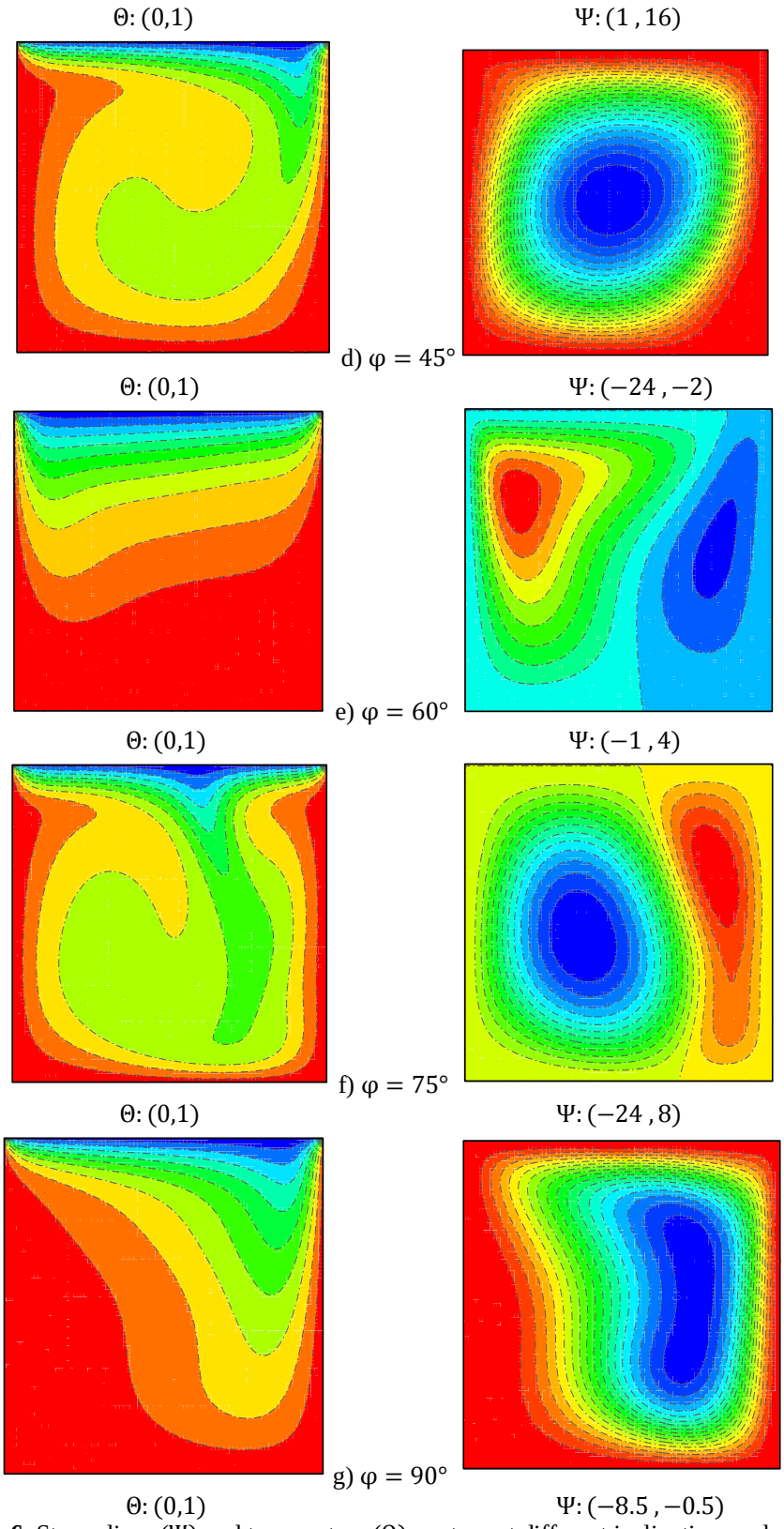

Fig.6: Streamlines (Ψ) and temperature (Θ) contour at different inclination angle for Ra= 10^5, RC = 10, $\omega = 0.5, \tau = 0.1$

To investigate the effect of radiation on the thermal behavior of cavity flow, the isotherm contours are sketched in Fig. 7, for two cases of pure convection (zero optical thickness) and combined radiation convection case. It is seen that the isotherm contours have similar patterns in these two cases. But the radiation effect causes a high temperature gradient near the active hot walls with the more uniform temperature at the core of the cavity because of penetration of the radiation of the hot wall into the medium. A similar study is done in Fig. 8, for the effect of radiation on flow patterns inside the cavity. It is depicted that in both cases, flow is bicellular with symmetry about the midplane, but the rate of fluid flow at the presence of radiation is greater than there is for pure convection. Distributions of convective and total Nusselt numbers along the bottom wall are presented in Fig. 9. The convective Nusselt number has its minimum value at two corners and the maximum value in the middle of the bottom wall. Fig. 9-a shows that the radiation effect causes an increase in the value of Nu_c because of the high temperature gradient near the active hot wall due to the penetration of radiative energy toward the medium. The total Nusselt number has a similar trend along the bottom wall, as it is illustrated in Fig. 9-b, such that there is a considerable increase in the value of Nu_t because of the radiation mechanism. The effect of the cavity inclination angle on both Nu_c and Nu_t distributions along the bottom wall is studied in Fig. 10. This figure shows a considerable effect of φ on the rates of convective and radiative wall heat fluxes. Maximum values of Nu_c and Nu_t occur for the cavity without inclination angle ($\varphi = 0$), and a sweep behavior is seen for both Nu_c and Nu_t by the variation of φ in the range of $0 < \varphi < 90$. In Fig. 11, distributions of Nu_c and Nu_t along the cavity bottom wall for three different values of Rayleigh numbers are presented. As it is expected, the value of the convective Nusselt number increases considerably with increasing Ra, as shown in Fig. 11-a. This is due to having high buoyancy forces in the natural fluid flow at high values of Ra that lead to stronger convective flow inside the cavity. But Fig. 11-b depicts that Ra does not have considerable influence on the radiative Nusselt number. Finally, the U and V velocity distributions at the vertical and horizontal mid-planes of the cavity at different cavity inclination angles are plotted in Fig. 12. Fig. 12-a shows low U-velocity components for the fluid flows that have symmetry about the midplane (X=L/2), for example, in the $\varphi = 0$ in which two similar vortices generate in the right and left parts of the cavity. For the inclination angles $\varphi = 30$ and $\varphi = 45$, Fig 12-a shows high values for U-velocity inside the cavity, especially near to the bottom and upper walls, while the inner core is rather stagnant. For the V-velocity profiles shown in Fig. 12, a complete symmetry about the vertical-cavity mid-plane is seen in the case of $\varphi = 0$. Besides all inclination angle in the range of $0 \leq \varphi \leq 90$, the high value of V-velocity takes place for cavity without inclination angle such that local maximum values occur near to the sidewalls and also at the vertical midplane. In the case of $\varphi = 60$, a buoyant flow with the minimum value for the V-velocity happens in the cavity, such that the inner core of the cavity is almost stagnant. Also, a sweep behavior for the V-velocity with inclination angle can be seen from Fig. 12-b in the range of $45 \leq \varphi \leq 90$.

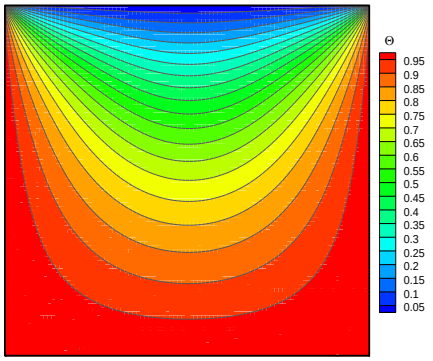

(a) : Pure convection

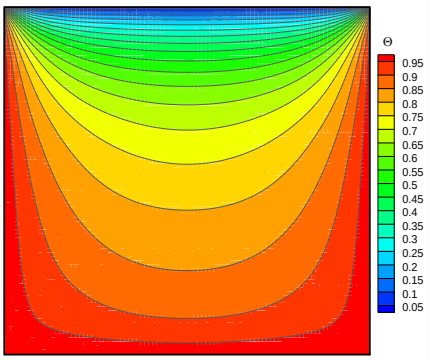

(b): Combined radiation and convection
(RC=20,$\tau = 1, \omega = 0.5, \varphi = 0$)

Fig.7: Distribution of the isotherm contours
$Ra = 10^3$. $Pr = 0.71$

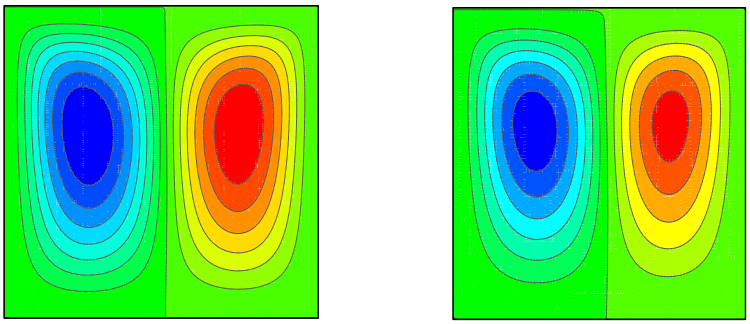

$\Psi: (-0.16\ , 0.16)$ $\Psi: (-0.2\ , 0.2)$

(a) : Pure convection (b) : Combined radiation and convection (RC=20,$\tau = 1.\ \omega = 0.5$)

Figure 8: Distribution of the streamlines
$Ra = 10^3. Pr = 0.71. = 0$

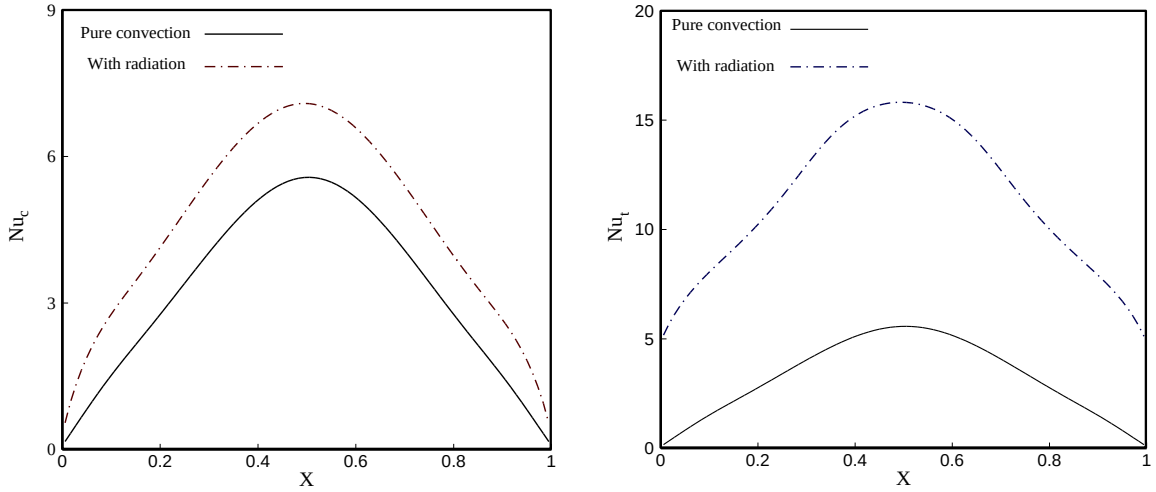

(a) Convective Nusselt number (b) Total Nusselt number

Fig.9: Distributions of Nu_c(a) and Nu_t(b) along the bottom wall
(RC=10,$\tau = 0.1$, Ra=10^5, $\omega = 0.5. \varphi = 0°$)

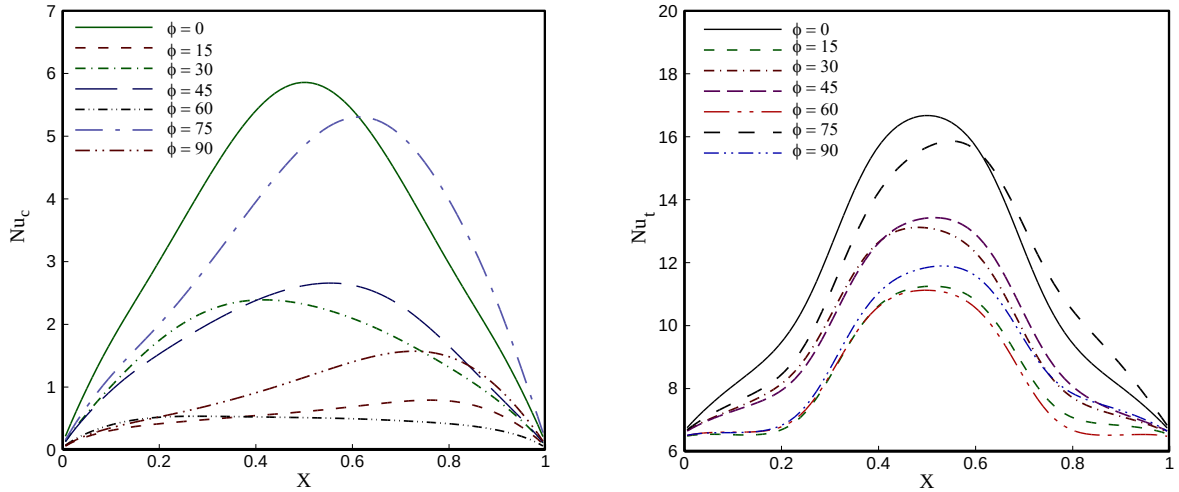

(a) Convective Nusselt number (b) Total Nusselt number

Fig.10: Distributions of Nu_c(a) and Nu_t(b) along the bottom wall
for the different inclination angle
(RC=10,$\tau = 0.1$, Ra=10^5, $\omega = 0.5$)

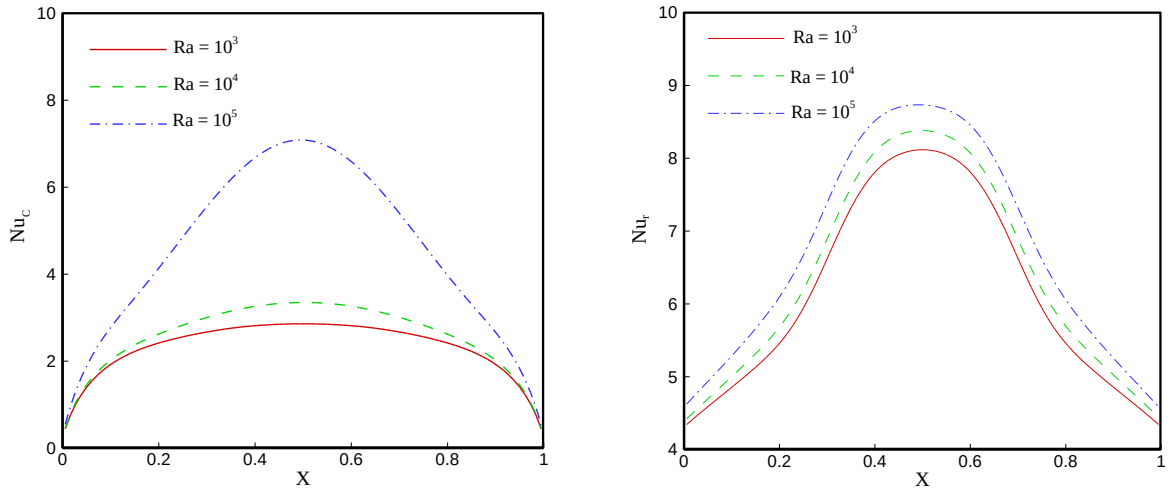

(a) Convective Nusselt number (b) Radiative Nusselt number

Fig.11: Distributions of Nu_c(a) and Nu_r(b) along the bottom wall for different Rayleigh number (RC=10,$\tau = 1$, $\omega = 0.5, \varphi = 0°$)

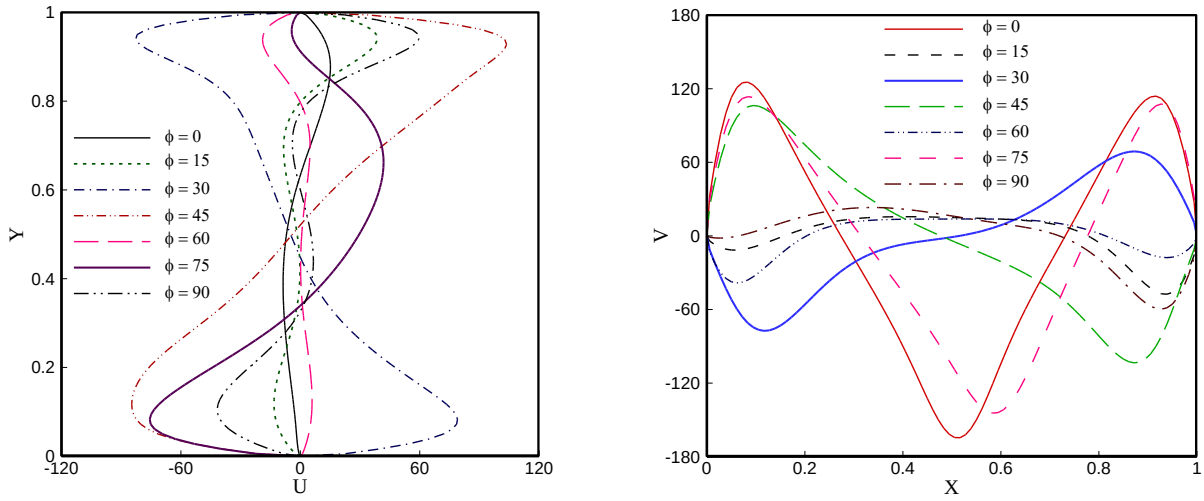

(a) U-velocity (b) V-velocity

Fig.12: U-velocity along the Y-axis (a) and V-velocity along the X-axis (b) for the different inclination angle (RC=10,$\tau = 0.1$, Ra=10^5, $\omega = 0.5$)

References

[1] Vahl Davis, G. "Natural convection of air in a square cavity: a comparison exercise", International Journal Numerical Methods Fluids, 3, pp. 227–248 (1983).

[2] Ostrach, S. "Completely confined natural convection", Developments in Mechanics, 10th Midwestern Mechanics Conference, 4, Johnson, Chicago Illinois, pp. 53-81 (1967).

[3] Ostrach, S. "Natural convection in enclosures", in Advances in Heat Transfer (edited by J. P. Hartnett and T. F. Irvine. Jr), 8, Academic Press, New York, pp. 161-227 (1972).

[4] Catton, I. "Natural convection in enclosures", In Heat Transfer, 6, National Research Council of Canada (1978).

[5] Markatos, N.C. and Pericleous, K.A. "Laminar and turbulent natural convection in an enclosed cavity",

International Journal of Heat Mass Transfer, 27, pp.755–772 (1984).

[6] Fusegi, T., Hyun, J.M., Kuwaharas, K. and Farouk, K. "A numerical study of three dimensional natural convection in a differentially heated cubical enclosure", International Journal of Heat Mass Transfer, 34, pp. 1543–1557 (1991).

[7] Chang, L.C., Yang, K.T. and Lloyd, J.R. "Radiation natural convection interaction in two-dimensional complex enclosures", ASME Journal Hear Transfer, 105, pp. 89-95 (1983).

[8] Webb, B.W. and Viskanta, R. "Radiation-induced buoyancy-driven flow in rectangular enclosures: experiment and analysis", ASME Journal Heat Transfer, 109, pp. 427-433 (1987).

[9] Yang, K.T. "Numerical modeling of natural convection radiation interactions in enclosures", In Heat Transfer 8th International Heat Transfer Conference, 1, Hemisphere, Washington, DC, pp. 131-140 (1986).

[10] Yucel, A., Acharya, S. and Williams, M.L. "Natural convection and radiation in a square enclosure", Numerical Heat Transfer A, 15, pp. 261-277 (1989).

[11] Lauriat, G. "Combined radiation–convection in gray fluids enclosed in vertical cavities", Journal Heat Transfer, 104, pp. 609–615 (1982).

[12] Lauriat, G. "Numerical study of the interaction of natural convection with radiation in nongray gases in a narrow vertical cavity", International Journal Heat Mass Transfer, pp. 153-158 (1982).

[13] Tan, Z., Howell, J.R. "Combined radiation and natural convection in a two dimensional participating square medium", International Journal Heat Mass Transfer, 34 (3), pp. 785–793 (1991).

[14] Moufekkir, F., Moussaoui, M.A., Mezrhab, A., Naji, H. and Lemonnier, D. "Numerical prediction of heat transfer by natural convection and radiation in an enclosure filled with an isotropic scattering medium", Journal of Quantitative Spectroscopy & Radiative Transfer, 113, pp. 1689-1704 (2012).

[15] Lari, K., Baneshi, M., Gandjalikhan Nassab, S.A, Komiya, A. and Maruyama, S. "Combined heat transfer of radiation and natural convection in a square cavity containing participating gases", International Journal of Heat and Mass Transfer, 54, pp. 5087-5099 (2011).

[16] Colomer, G., Costa, M., Consul, R. and Oliva, A. "Three-dimensional numerical simulation of convection and radiation in a differentially heated cavity using the discrete ordinate method", International Journal of Heat and Mass Transfer, 47, pp. 257-269 (2004).

[17] Capdevila, R., Lehmkuhl, O., Colomer, G. and Perez-Segarra, C.D. "Study of turbulent natural convection in a tall differentially heated cavity filled with either non-participating, participating grey or participating semigrey media", J. Phys: Conf. Ser. 395 012155 (2012).

[18] Capdevila, R., Lehmkuhl, O., Trias, F.X., Perez-Segarra, C.D. and Colomer, G. "Turbulent natural convection in a differentially heated cavity of aspect ratio 5 filled with non-participating and participating grey media", J. Phys: Conf. Ser. 318 042048 (2011).

[19] Capdevila, R., Perez-Segarra, C.D. Lehmkuhl, O. and Colomer, G. "Numerical simulation of turbulent natural convection and gas radiation in differentially heated cavities using FVM, DOM and LES", 6th International Symposium on Radiative Transfer, Antalya, Turkey (2010).

[20] Ibrahim, A., Saury, D. and Lemonnier, D. "Coupling of turbulent natural convection with radiation in an air-filled differentially-heated cavity at Ra $=1.5\times10^{9}$", Computers and Fluids, 88, pp. 115–125 (2013).

[21] Baytas, A.C. "Entropy generation for natural convection in an inclined porous cavity", International Journal Heat Mass Transfer, 43, pp. 2089–2099 (2000).

[22] Oztop, H.F. "Natural convection in partially cooled and inclined porous rectangular enclosures", International

Journal of Thermal Science, 46, pp. 149–156 (2007).

[23] Varol, Y., Oztop, H.F., Koca, A. and Özgen, F. "Natural convection and fluid flow in inclined enclosure with corner heater", Applied Thermal Engineering, 29, pp. 340–350 (2009).

[24] Bouali, H., Mezrhab, A., Amaoui, H. and Bouzidi, M. "Radiation-natural convection heat transfer in an inclined rectangular enclosure", International Journal of Thermal Science, 45, pp. 553-566 (2006).

[25] Ahmed, S.E, Oztop H.F. and Al-Salem, K. "Natural convection coupled with radiation heat transfer in an inclined porous cavity with corner heater", Computers and Fluids, 102, pp. 74-84 (2014).

[26] Mezrhab, A., Bouali, H. and Abid, C. "Radiation-natural convection interactionsin an enclosures with a heat-generating conducting body", Congress Francis de Thermique SFT, pp. 25-28 (2004).

[27] Mezrhab, A., Bouali, H. and Abid, C. "Modeling of combined radiative and convective heat transfer in an enclosure with a heat-generating conducting body", International Journal Computer Methods, 2(3), pp. 431-450 (2005).

[28] Moein Addini, M., Gandjalikhan Nasab A. "Combined mixed convection and radiation simulation of inclined lid driven cavity", Energy Equipment and Systems, 6(3), pp.261-277(2018).

[29] Rabhi, M., Bouali, H. and Mezrhab, A. "Radiation-natural convection heat transfer in inclined rectangular enclosures with multiple partitions", Journal of Energy Conversion and Management, 49, pp. 1228-1236 (2008).

[30] Patankar S.V. "Numerical Heat Transfer and Fluid Flow", Hemisphere Publishing, Washington, DC (1980).

[31] Modest, M. F., 2003, Radiative Heat Transfer, Academic, San Diego, CA, Chap. 16.

[32] Patankar, S.V. "Numerical Heat Transfer and Fluid Flow", Taylor & Francis, Philadelphia, PA, Chap. 7 (1981).

[33] Byun, K.H. and Hyuk, Im. M. "Radiation-laminar free convection in a square duct with specular reflection by absorbing-emitting medium", KSME International Journal, 16(10) pp. 1346-1354 (2002).

[34] Mahapatra, S.K., Dandapat, B.K. and Sarkar, A. "Analysis of Combined Conduction and Radiation Heat Transfer in Presence of Participating Medium by the Development of Hybrid Method", Journal of Quantitative Spectroscopy & Radiative Transfer, 102, pp. 277–292 (2006).